RSC Advances

PAPER

View Article Online
View Journal | View Issue

Cite this: *RSC Adv.*, 2021, **11**, 10416

Ultra-high thermally stable gold nanorods/radial mesoporous silica and their application in enhanced chemo-photothermal therapy†

Chun Shan,[a] Yuting Huang,[a] Junhao Wei,[b] Min Chen *[a] and Limin Wu [a]

Received 11th January 2021
Accepted 22nd February 2021

DOI: 10.1039/d1ra00213a

rsc.li/rsc-advances

In this work, gold nanorods embedded in ultra-thick silica shells with radial mesopores (AuNR/R-SiO_2) were successfully synthesized in an ethanol/water solution. By optimizing the concentration of CTAB and the volume of ethanol, a shell thickness up to 83 nm was realized. Taking advantage of the ultra-thick silica shell, AuNR/R-SiO_2 exhibited ultra-high thermal stability—could retain the integrity and photothermal effects even after 800 °C thermal annealing, providing inspiring sights into the application under some extreme conditions. After continuous irradiation for twenty times, the photothermal effects of AuNRs coated with R-SiO_2 still remained perfect without performance degradation and shape change. Besides, abundant mesopores could effectively improve the photothermal conversion efficiency of AuNRs. AuNR/R-SiO_2 exhibited an outstanding loading capacity up to 2178 mg g^{-1} with doxorubicin (DOX) as the model drug, and the release behaviors could be nicely controlled by acidity and near-infrared (NIR) laser to achieve the "On-demand" mode. *In vitro* experiments showed that AuNR/R-SiO_2 were biocompatible and easy to be internalized by HeLa cells. In addition, due to the ultra-thick silica shell, the effect of the combined chemo-photothermal therapy using AuNR/R-SiO_2/DOX was significantly enhanced, showing a higher therapeutic efficiency than single chem- or photothermal therapy. It was worth noting that AuNR/R-SiO_2 are effective and promising for drug delivery and tumor therapy.

1 Introduction

Gold nanorods (AuNRs) have been widely studied as popular photothermal therapy agents owing to their good biocompatibility, unique and tuneable localized surface plasmonic response (LSPR) and photothermal effects.[1–3] Under the irradiation of a near-infrared (NIR) laser, AuNRs with LSPR located at the NIR region (650–950 nm) show an excellent light absorption property and can effectively convert light into heat.[4] However, when the NIR light penetrates deep into tumors, the energy will gradually decrease due to light scattering and absorption, which is insufficient to be a cancer cell killer.[5] Therefore, the synergetic combined chemo-photothermal therapy in a single AuNR platform for cancer treatment has aroused extensive attention.

As promising anticancer-drug carriers, gold nanorods are still imperfect. First, the high surface tension causes low thermal stability, although the optical properties of AuNRs can be easily achieved during synthesis under mild reaction conditions. However, it is very critical to ensure that the performance of AuNR/R-SiO_2 still remains perfect under high temperature conditions. When irradiated repeatedly or heated at a high temperature, AuNRs tend to be transformed into large or small spherical nanoparticles *via* surface melting to reduce their surface tension, resulting in the change of rod shape and the degradation of photothermal effects.[6] In order to improve the thermal stability of AuNRs, many efforts have been made such as coating with titanate (for detection of H_2, 400 °C),[7] thin silica (for plasmon-enhanced photoconductivity, 600 °C)[8] and encapsulation in yttria-stabilized zirconia (high-temperature plasmonic sensing, 600 °C).[9] These methods still have some disadvantages such as limited thermal treating temperatures and damaged LSPR properties. Therefore, there still remain challenges to develop an effective and easy method to improve the thermal stability of AuNRs.

Second, the specific surface area of AuNRs is relatively low, resulting in the limitation of the loading amount and the size of guests. Generally, in order to improve the efficiency of combined therapy, a large laser power intensity and a high injection dose are adopted, which will increase the risk of therapy.[10–12] It is critical to choose a suitable nano-drug carrier to achieve better therapeutic effects. In an effort to overcome these disadvantages, the surface of AuNR is conjugated with various coatings such as polymers,[13–15] mesoporous silica,[16,17] metal–organic frameworks,[18,19] and liposomes.[20,21] Among them, AuNR coated with the mesoporous silica shell (AuNR/

[a]*Department of Materials Science, State Key Laboratory of Molecular Engineering of Polymers, Fudan University, Shanghai, 200433, China. E-mail: chenmin@fudan.edu.cn*

[b]*School of Life Sciences and Technology, Tongji University, Shanghai, 200092, China*

† Electronic supplementary information (ESI) available. See DOI: 10.1039/d1ra00213a

SiO_2) exhibited a great potential to realize chemo-photothermal therapy due to their uniform pore size, high biocompatibility, and easy surface functionalization.[22–24] However, according to the classical protocol reported by Gorelikov,[25] the thickness of the silica shell is only ~30 nm with disordered mesopores of ~4 nm diameter, which cannot provide enough space for cargos, thereby limiting the size of the guests. As to improve the drug loading capacity, much work so far has focused on the "layer-by-layer" method[25] to increase the shell thickness, or "surface-protected etching" to produce the hollow structure.[26,27] However, the loading capacity is still limited.

In this work, we first developed a flexible and controlled strategy to fabricate sphere-like AuNR/radial silica (AuNR/R-SiO_2) with a thicker silica shell (~83 nm) and larger pores (~4.8 nm). After thermal annealing at different temperatures (up to 800 °C), AuNRs embedded in this core–shell structure still retained the rod-like shape and good photothermal effects, indicating the ultra-high thermal stability. After continuous irradiation for twenty times, the photothermal effects of AuNRs coated with R-SiO_2 still remained perfect without performance degradation and shape change. Besides, the abundant mesopores could effectively improve the photothermal conversion efficiency of AuNRs. Owing to the thicker shell and larger pore size, the loading capacity of doxorubicin (DOX) in the AuNR/R-SiO_2 spheres was relatively high as 2178 mg g^{-1} and the release behaviours could be nicely controlled by acidity and NIR laser, achieving drug release on demand. The HeLa cell experiments exhibited that due to the ultra-thick silica shell, the treatment effect of the combined chemo-photothermal therapy using AuNR/R-SiO_2/DOX was significantly enhanced and showed a more effective therapeutic effect for cancer therapy than other reports.

2 Experimental section

2.1. Materials

Sodium borohydride ($NaBH_4$, 98%), hydrogen tetrachloroaurate trihydrate ($HAuCl_4 \cdot 3H_2O$, ≥99.9%), L-(+)-ascorbic acid (AA, ≥99%), silver nitrate ($AgNO_3$, ≥99%), tetraethyl orthosilicate (TEOS), aqueous ammonia solution ($NH_3 \cdot H_2O$, 25–28%) and doxorubicin hydrochloride (DOX) were received from ALADDIN Reagent (Shanghai) Co., Ltd. Hydrochloride solution (HCl, 36–38%) and cetyltrimethylammonium bromide (CTAB, ≥99%) were obtained from Sinopharm Chemical Reagent Co., Ltd. Absolute ethanol (EtOH, ≥99.7%) was acquired from Shanghai Titan Technology Co., Ltd. Deionized water (~18.2 MΩ) was used in all preparation procedures.

2.2. Characterizations

A transmission electron microscope (TEM) from Tecnai G2 20 TWIN, America, operating at an accelerating voltage of 200 kV was used. The surface area and pore volume were calculated by the Brunauer–Emmett–Teller (BET) analysis (relative pressure range from 0.0 to 1.0). The Barrett–Joyner–Halenda (BJH) analysis was used to calculate the pore size distribution from the absorption branches. A UV-vis-NIR spectrophotometer (U-4100, HITACHA, Japan) was adopted to record UV-vis-NIR spectra. Fluorescence intensities were tested using a QM40 fluorescence spectrometer (PTI). Elemental distribution was obtained by energy-dispersive X-ray spectroscopy (EDS, X-Max 80T, America) at an accelerating voltage of 200 kV. Zeta potentials and hydrodynamic diameters were measured using a Zetasizer Nanoseries (Nano ZS90, Malvern).

2.3. Synthesis of AuNRs

Gold nanorods (AuNRs) were prepared following the procedure in the published report with minor modifications.[17] First, the chemical reduction of $HAuCl_4$ using fresh $NaBH_4$ was adopted to prepare CTAB-capped gold seeds. In a typical formulation, aqueous $HAuCl_4$ (5.0 mL, 0.5 mM) was mixed with a CTAB solution (5.0 mL, 0.2 M). Then, fresh ice-cold $NaBH_4$ (0.6 mL, 0.01 M) was introduced to the solution under vigorous stirring at 26 °C. Two minutes later, the solution was kept un-disturbed for 2 h to guarantee the complete degradation of residual $NaBH_4$.

Next, the AuNRs were synthesized from the gold seeds in the growth solution. To prepare the growth solution, a CTAB solution (100 mL, 0.1 M) was mixed with HCl (3.0 mL, 1 M), $AgNO_3$ (1.0 mL, 10 mM) and $HAuCl_4$ (2.0 mL, 25 mM). After stirring well, ascorbic acid (0.7 mL, 0.0788 M) was added and the mixture became colourless immediately. Last, 120 μL gold seeds were added. After vigorous stirring for a while, the solution was kept un-disturbed at 29 °C overnight. In order to separate AuNRs from excess CTAB, the solution was centrifuged and washed with water. AuNRs with an LSPR band at 776 nm were obtained. By controlling the amount of $AgNO_3$ and HCl, AuNRs were prepared with different LSPR bands from 733 nm to 898 nm.

2.4. Synthesis of AuNR/R-SiO_2

Mesoporous silica-coated AuNRs with radial pores (AuNR/R-SiO_2) were prepared according to Marta N. Sanz-Ortiz with some modifications.[28] First, centrifugal washing was used to remove the CTAB surfactants around AuNRs before re-dispersion in 5 mL water. Meanwhile, a CTAB solution (170 mL, 10 mM) was mixed with 70 mL EtOH at 30 °C. Second, the AuNRs were transferred into the above mixture. After stirring for 1 h to make equilibration, 0.5 mL NH_4OH (25–28%) was introduced and stirred for 5 min to ensure the homogeneity of the solution. Then, the TEOS ethanol solution (1 : 1 v/v) was gradually injected into the mixture for 6 h (injection rate: 0.2 mL h^{-1}) under vigorous stirring. The mixture reacted at 60 °C for 1 day to get the final product AuNR/R-SiO_2. By adjusting the CTAB concentration and EtOH volume, AuNR/R-SiO_2 different sizes, shapes and morphologies were obtained.

2.5. Thermal annealing

AuNR/R-SiO_2 with LSPR at 935 nm were dried at 40 °C, and then, the powder was thermally annealed in a tube furnace under the flow of Ar. The temperature increased from 30 °C to the setting temperature (400, 500, 600, 700 and 800 °C) and then kept for 1 h. After that, the powder was cooled to room temperature.

2.6. Photothermal characterization after thermal annealing

AuNR/R-SiO_2 after thermal annealing at different temperatures were dispersed into an aqueous solution and then added to

a centrifuge tube (500 μL). A 808 nm NIR laser (2.0 W cm^{-2}, 8 min) was adopted to irradiate each tube, and at the same time, a near-infrared camera (FLIR-T62101, Sweden) was adopted to record the solution temperature every 20 s.

To investigate the change in the photothermal conversion capacity of AuNR/R-SiO_2 with the increase in irradiation frequency, the AuNR/R-SiO_2 solution was irradiated repeatedly for twenty times. The photothermal conversion efficiency (η) was calculated as follows:[29]

$$\eta = \frac{hS(T_{max} - T_{surr}) - Q_{dis}}{I\left(1 - 10^{-\lambda 808}\right)} \quad (1)$$

$$hS = \frac{m \times C_{H_2O}}{\tau_s} \quad (2)$$

In eqn (1), h (W m^{-2} K^{-1}) is the heat transfer coefficient, S (m^2) is the container surface area, T_{max} (K) is the highest temperature of AuNR/R-SiO_2 within 8 min, T_{surr} (K) is the ambient temperature (25 °C), Q_{dis} (W) is the heat generated by solvent and container under the same irradiation condition, I (W) is the laser power, and λ_{808} is the absorbance intensity of AuNR/R-SiO_2 at 808 nm. In eqn (2), m (g) is the mass of the solution, C_{H2O} [J $(g\ K)^{-1}$] is the heat capacity of water, and τ_s (s) is the time constant.[30]

2.7. Drug loading and release

These experiments were conducted according to our previous work.[31,32] Before drug loading, AuNR/R-SiO_2 were first thermally annealed to completely remove residual CTAB. After that, 2 mg of them was added into the DOX solution at different concentrations (0.125, 0.25, 0.5, 1.0, 1.25, and 1.5 mg mL^{-1}) and stirred at 25 °C for 24 h in the darkness. Finally, in order to remove the unloaded-DOX, the DOX-loaded AuNR/R-SiO_2 (AuNR/R-SiO_2/DOX) were washed three times with water. For calculating the loading capacity and efficiency, the supernatant DOX solution was collected and measured according to the UV-vis (the absorption spectra of DOX was 480 nm, $y = 20.763x + 0.052$, $R^2 = 0.9992$, Fig. S1†) to calculate the amounts of loaded drugs. The formula is as follows: loading capacity (DOX) = amounts of loaded DOX/weight of AuNR/R-SiO_2, loading efficiency (%) = amounts of loaded DOX/initial amount of DOX × 100%.

Drug release behaviours of AuNR/R-SiO_2/DOX were performed by acidity and NIR laser stimuli. Typically, the samples were diluted with 4 mL PBS at different pH levels (7.4 and 5.0) at 37 °C. After stirring for a while, the solutions were irradiated with 2 W cm^{-2} NIR laser for 5 min at fixed time points. After centrifugation, the supernatants were collected to calculate the amount of released DOX followed by re-adding fresh PBS. The formula is as follows: relative release (%) = amount of released DOX/amounts of loaded DOX × 100%.

2.8. Intracellular drug release visualized by confocal laser scanning microscopy (CLSM)

HeLa cells (5000 cells per well) were seeded in a 96-well plate. After incubation for 24 h, the cells were treated with free DOX and AuNR/R-SiO_2/DOX (at the same DOX feeding concentration) for another 4 h. Then, the cells with AuNR/R-SiO_2/DOX were irradiated with 2 W cm^{-2} 808 nm NIR laser for 5 min. After incubation for 24 h, the cells were washed with PBS and incubated with DAPI/PBS buffer solution at room temperature for 15 min in the darkness. After washing with PBS for further three times, 200 μL PBS was added. The CLSM was used to qualitatively analyse pH- and NIR-triggered drug release within the cell culture. The DOX molecules and cell nuclei were distinguished by red signal fluorescence and blue signal fluorescence (DAPI).

2.9. Cytotoxicity of blank nanocarriers

The evaluation of the biological non-toxicity of blank nanocarriers was conducted by Cell Counting Kit-8 (CCK-8). HeLa cells (5000 cells per well) were cultivated in a 96-well plate. Then, the fresh medium containing different AuNR/R-SiO_2 concentrations (0, 10, 20, 40, 100, 200, 300 and 400 μg mL^{-1}) was added and cultured for 24 h. Then, the CCK-8 solution (100 μL) was introduced into wells. After incubation for another 4 h, a microplate reader was adopted to test the absorbance at 450 nm of each well.

2.10. Combined chemo-photothermal therapy

HeLa cells (5000 cells per well) were cultivated in a 96-well plate. After incubation for 24 h, free DOX, AuNR/R-SiO_2, and AuNR/R-SiO_2/DOX (with the equivalent DOX concentration: 0.01, 0.1, 0.2, 0.5, 1.0, 2.5 and 5.0 μg mL^{-1}) were added and incubated for another 4 h. For chemotherapy only, cells were cultured without NIR irradiation; to achieve photothermal therapy, cells were irradiated with 808 nm laser at 2.0 W cm^{-2} for 5 min and incubated for 20 h. The CCK-8 solution (100 μL) was introduced into wells and incubated for 4 h. At last, the cell viability was tested *via* a standard CCK-8 assay. Each experiment was conducted three times.

3 Results and discussion

3.1. Synthesis and characterization of AuNR/R-SiO_2

AuNRs with an aspect ratio of ~4.1 (54 × 14 nm^2) were prepared by the seed-mediated growth method (Fig. 1a). Different from the dense silica shell deposited onto AuNRs by the classic Stöber method,[25] a porous out layer was fabricated directly without further modification (Fig. 1b). As shown in Fig. 1c, AuNRs were coated with a clear mesoporous silica shell, and the pores extended radially from the centre to the surface of particles. In addition, the shell thickness was up to ~83 nm, which was higher than the previous work (~30 nm),[26,27] offering more accommodation for guest loading. Moreover, the TEM images showed that AuNR/R-SiO_2 had a size of ~174 nm in length and ~150 nm in width with a shorter aspect ratio (~1.16) and narrow size distribution (Fig. S2†). These results indicated that AuNRs with radial mesoporous silica coating were successfully prepared. The BET analysis of the AuNR/R-SiO_2 by N_2 adsorption–desorption isotherm is presented in Fig. 1d. The surface area, pore volume and average pore diameter were measured to be 934.33 m^2 g^{-1}, 0.69 cm^3 g^{-1} and 4.8 nm, respectively, significantly higher than the most recent results.

The synthesis of AuNR/R-SiO_2 involves two steps: first, AuNRs were prepared and then introduced into the growth conditions of mesoporous silica. During the whole preparation process, CTAB

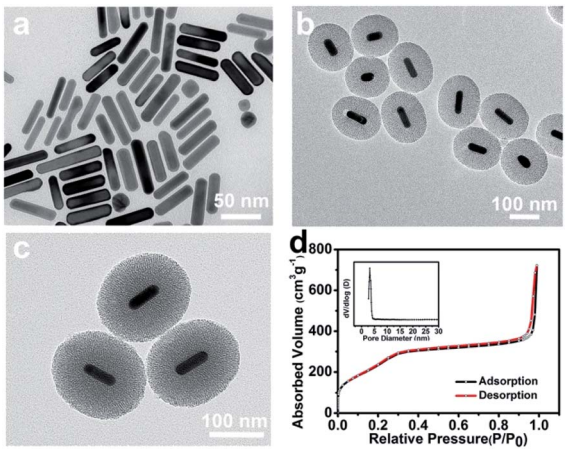

Fig. 1 TEM images of (a) AuNR; (b) AuNR/R-SiO_2; (c) magnification of AuNR/R-SiO_2 and (d) N_2 adsorption–desorption isotherm curves of AuNR/R-SiO_2 and their corresponding pore size distribution (inset).

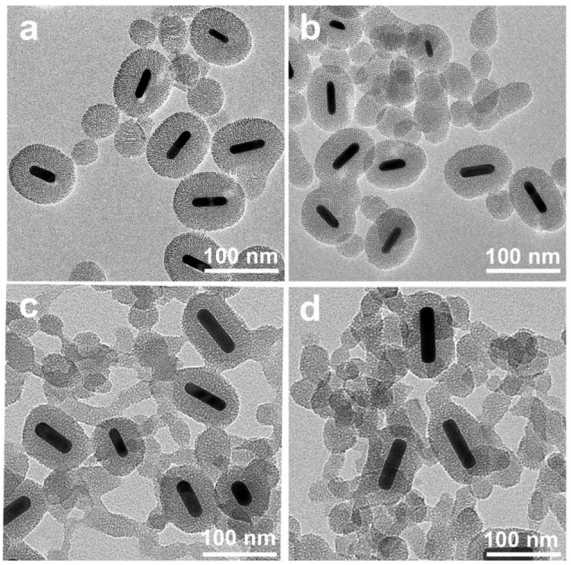

Fig. 2 TEM images of AuNR/R-SiO_2 were collected at different concentrations of CTAB. (a) 20 mM; (b) 30 mM; (c) 40 mM; and (d) 50 mM. Volume of EtOH: 75 mL.

are of great importance. First, it acts as the structure directing agent to prepare rod-like AuNRs, and then as the surfactant surrounding the surface of AuNRs *via* electrostatic interactions, so that AuNRs can be stably dispersed in the aqueous solution.[33] Third, CTAB bilayer around AuNRs acts as a site for silica nucleation[34] to form the core shell structure. Beyond that, they also served as the soft template to produce the mesoporous structure.

In this work, AuNR/R-SiO_2 with different shapes, sizes and morphologies were obtained by changing the concentration of CTAB. When the CTAB concentration was lower than 10 mM, the reaction solution turned to be colourless, indicating the aggregation and precipitation of AuNRs. That is because CTAB are easy to be removed from the AuNR surface to the bulk solution due to their high solubility in ethanol, which would destroy the stability of the colloidal nanorod. As the CTAB concentration increased from 20 mM to 50 mM, the shell thickness and aspect ratio changed from 33 nm to 20 nm, and 1.26 to 1.6, respectively (Fig. 2 and S3a†). With the higher concentration, more CTAB are free in the solution, providing a template for silica nucleation. Accordingly, the shell thickness would decrease and more by-product mesoporous silica sphere would be prepared. Hence, it is critical to properly adjust the CTAB concentration to minimize nanoparticle precipitation and increase the shell thickness, generally at least above the critical micelle concentration.[35,36]

To verify this assumption, the dependence on the EtOH volume was further investigated (Fig. S3b and S4†). By increasing the volume of EtOH from 35 mL to 70 mL, more CTAB were dissolved, the diameter and shell thickness increased from 83 nm to 174 nm, and 19 nm to 83 nm, respectively. Above all, in order to optimize the conditions for the incorporation of AuNRs into mesoporous silica, the CTAB concentration and ethanol/water volume should be strictly adjusted.

3.2. Thermal stability of AuNR/R-SiO_2

During thermal annealing, AuNRs will transform from rods into spherical particles because the high surface tension will drive the nanoparticles to reduce their surface-to-volume ratio.[8] In this circumstance, the LSPR band of AuNR/R-SiO_2 tends to blue-shift until it disappears[6] because of the decrease in the aspect ratio. Hence, the LSPR peak is adopted to monitor the structural change so as to investigate the thermal stability of AuNR/R-SiO_2. In this work, AuNRs with higher LSPR at 898 nm were synthesized. After coating with a 80.4 nm-thick silica shell, the LSPR peaks exhibited a red-shift from 898 nm to 935 nm obviously (Fig. S5†) with the increase in refractive index near AuNRs.

Fig. 3 shows the UV-vis-NIR absorption spectra of AuNR/R-SiO_2 before and after thermal annealing at different temperatures. Even after heating at 800 °C, there still exist two distinct peaks: a localized TSPR peak at 520 nm and different LSPR peaks, confirming that AuNRs incorporated into the ultra-thick silica shell maintained the rod-like structure. As can be seen, after thermal annealing at 400 °C to 800 °C for 1 h, LSPR with original 935 nm blue-shifted from 859 nm to 818 nm obviously, indicating the reduction in the aspect ratio. This conclusion is in accordance with the observation from TEM images (Fig. 4 and Table S1†): the length of AuNRs decreased from 72.8 nm to 60.8 nm; meanwhile, the width of AuNRs increased from 13.4 nm to 16.0 nm, and the aspect ratio reduced from 5.5 to 3.8. Although the dimension of AuNRs changed, their shape still remained rod-like and retained the integrity after heating and only some small cracks appeared on the surface of silica shell. These results indicated that the ultra-thick solid silica shell can extremely improve the thermal stability of AuNRs up to 800 °C and prevent the structural change from rod to sphere, which broaden the application of AuNRs under extreme conditions.

In order to trace the change regularity of LSPR and TSPR before and after thermal annealing at different temperatures, SPR peaks at different temperatures are shown in Fig. 5. It is worthwhile mentioning the LSPR peak was a linear variation

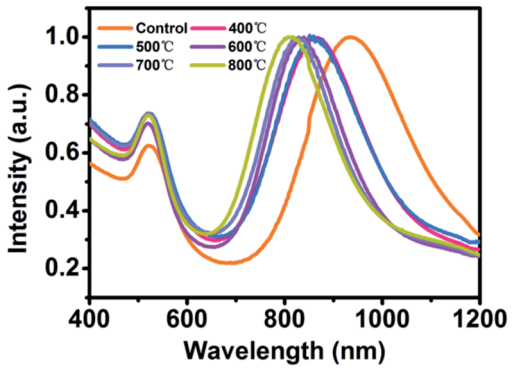

Fig. 3 UV-vis-NIR absorption spectra of AuNR/R-SiO_2 before and after thermal annealing at different temperatures: 400 °C, 500 °C, 600 °C, 700 °C and 800 °C.

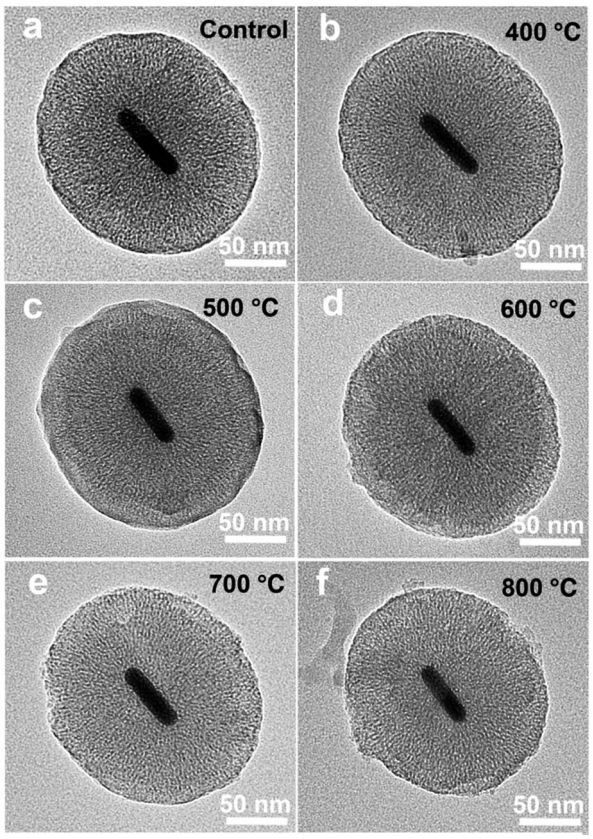

Fig. 4 TEM of AuNR/R-SiO_2 before and after thermal annealing at different temperatures: 400 °C, 500 °C, 600 °C, 700 °C and 800 °C.

with the heating temperature from 400 to 800 °C ($y = -0.1045x + 901.7$, $R^2 = 0.997$). This may cast a new light on the application of AuNR/R-SiO_2—based on this formula, on the one hand, one can infer their thermal history by measuring the LSPR peaks after heating. On the other hand, in some high temperature for device fabrication or application conditions, AuNRs with higher LSPR can be prepared first and then the LSPR could be adjusted to the specified peaks by thermal annealing. For example, in this work, thermal annealing was adopted to completely remove the residual CTAB of AuNR/R-SiO_2 instead of the time-consuming and repeated ion exchange way;[16] after this high temperature processing, the optical properties of AuNRs still remained perfect and could be used in drug release and photothermal therapy.

In addition, in order to verify the shape stability of AuNRs embedded in the ultra-thick silica shell during the photothermal heating process, the AuNR/R-SiO_2 solution was irradiated repeatedly for twenty times, which is more than that reported in similar studies. As shown in Fig. 6, after continuous irradiation of AuNR/R-SiO_2 for twenty times, the LSPR peak showed almost no change and AuNRs still retained the rod-like structure. These results indicated that the ultra-thick silica shell can effectively preserve the LSPR and shape of AuNRs, enhancing the shape stability of AuNRs during photothermal heating.[37]

3.3. Photothermal characterization of AuNR/R-SiO_2 after thermal annealing

AuNRs can convert NIR light into heat with high efficiency. In order to verify the photothermal effects of the products, original AuNR/R-SiO_2 as well as the corresponding thermal treated samples were irradiated with an 808 nm laser (2.0 W cm^{-2}). The maximum temperature and their corresponding LSPR are shown in Table 1. As shown in Table 1 and Fig. 7a, the temperature of original AuNR/R-SiO_2 increased from 25 °C to more than 60 °C within 8 min, and with the increase in thermal annealing temperature, the maximum temperature of the samples also increased even up to 89.7 °C after post-treatment at 800 °C. That is because after heating at different temperatures, the LSPR obviously blue-shifted from 935 nm to 818 nm, which is gradually close to 808 nm, resulting in a higher efficiency in photothermal conversion. Beyond that, the photothermal effects of AuNR/R-SiO_2 after thermal annealing at 800 °C were dose and laser intensity-dependent (Fig. 7b and c). When irradiated with a 2 W cm^{-2} NIR laser, the temperature would increase by 12.3 °C to 35.6 °C, as the concentration of AuNR/R-SiO_2 increased from 50 to 250 μg mL^{-1}. When increasing the laser intensity from 1.0 W cm^{-2} to 2.0 W cm^{-2}, the temperature would increase by 21.5 °C to 46.6 °C at 250 μg

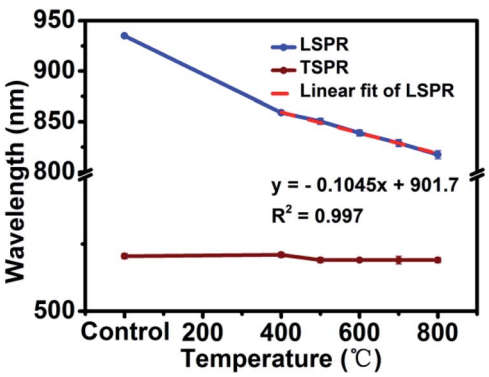

Fig. 5 LSPR and TSPR of AuNR/R-SiO_2 before and after thermal annealing at different temperatures: 400 °C, 500 °C, 600 °C, 700 °C and 800 °C.

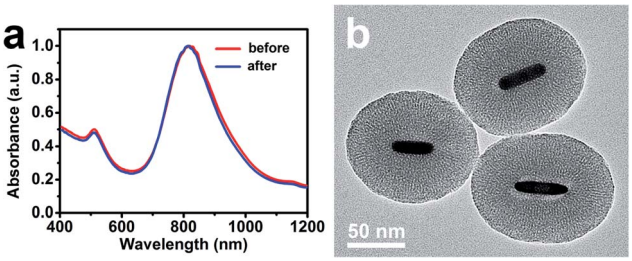

Fig. 6 (a) UV-vis-NIR absorption spectra of AuNR/R-SiO_2 before and after continuous irradiations for twenty times. (b) TEM of AuNR/R-SiO_2 after continuous irradiations for twenty times.

mL^{-1}. Furthermore, the photothermal stability of AuNR/R-SiO_2 was also investigated (Fig. 7d). The AuNR/R-SiO_2 after heating at 800 °C was irradiated four times "on/off" cycles. It could be observed that the photothermal effect did not show much change except that the T_{max} value decreased slightly with repeating irradiation (from 87.1 °C at the 1st time to 80.9 at the 4th time), which means the negative effect of heat history on photothermal conversion. Considering that 43 °C is high enough for moderate hyperthermia to effectively kill cancer cells with minimal side effects on normal cells nearby,[38,39] the present AuNR/R-SiO_2 after thermal annealing still have excellent photothermal effects and offer exciting opportunities to be applied under high temperature conditions.

3.4. Photothermal characterization of AuNR/R-SiO_2 after continuous irradiation of AuNR/R-SiO_2

In order to verify the change in the photothermal conversion capacity of AuNR/R-SiO_2 with the increase in irradiation frequency, the AuNR/R-SiO_2 solution was repeatedly irradiated twenty times with a 2.0 W cm^{-2} 808 nm NIR laser. As shown in Fig. 8, the photothermal conversion curve of AuNR/R-SiO_2 remained substantially unchanged during the whole process. According to our previous report, in *in vivo* experiments, the nano-drug carriers will accumulate in tumor tissues for 6–8 h because of enhanced permeability and retention (EPR) effects.[23] Therefore, AuNR/R-SiO_2 can achieve repeated photothermal therapy in the limited time without the degradation of photothermal effects, which will improve the utilization of nano-drug carriers.

In addition, the photothermal conversion efficiency (η) was also measured to evaluate the potential application as photothermal therapy agents (Fig. S6†). According to the calculation results, the η value remained stable around 70%, which is significantly higher than that of AuNRs (22%).[40] This is because the mesopore structure of the SiO_2 shell could effectively suppress the light reflection and enhance the light absorption of AuNRs.[37,41] Thanks to the high surface area (934.33 m^2 g^{-1}) and pore volume (0.69 cm^3 g^{-1}) of the ultra-thick mesoporous shell, the photothermal effect of AuNRs could be extremely improved by the ultra-thick silica layer.

Table 1 The maximum temperature (T_{max}) of AuNR/R-SiO_2 after exposed to 808 nm laser at 2.0 W cm^{-2} for 8 min and their corresponding LSPR after heated at different temperature for 1 h

Temperature (°C)	LSPR (nm)	T_{max} (°C)
Control	935.0	60.5
400	859.0	75.8
500	850.5	81.1
600	839.0	84.8
700	829.0	89.5
800	817.5	89.7

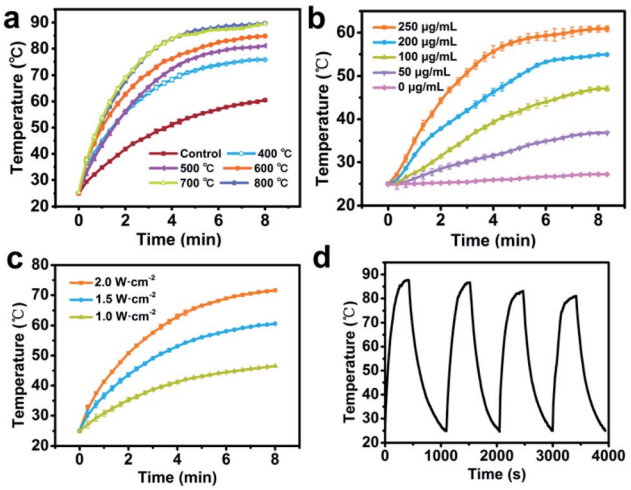

Fig. 7 (a) Temperature rise of the AuNR/R-SiO_2 solution before and after thermal annealing upon irradiation at 2.0 W cm^{-2} 808 nm laser intensity; temperature rise of AuNR/R-SiO_2 (800 °C) solution of (b) different concentrations upon 2.0 W cm^{-2} 808 nm laser irradiation; (c) different power intensity at 250 μg mL^{-1} and (d) for four repeated irradiation cycles.

3.5. Drug loading capacity

To achieve controllable drug release for chemo-therapeutics and provide hyperthermal cancer therapy for obtaining better therapeutic efficiency, AuNR/R-SiO_2 after thermal annealing at 800 °C with LSPR at 818 nm served as an anticancer-drug carrier. By simply mixing the DOX solution with AuNR/R-SiO_2, drugs were loaded into the radial mesopores *via* electrostatic

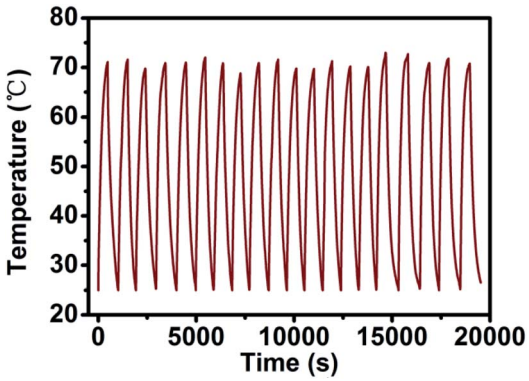

Fig. 8 Photothermal conversion curve of AuNR/R-SiO_2 for twenty repeated irradiation cycles.

interactions (Fig. S7a,† the ζ-potential of AuNR/R-SiO_2 is −22.5 mV, while DOX is positively charged). Compared with free AuNR/R-SiO_2, a clearly new absorption peak at 480 nm emerged in the UV-vis-NIR spectra of the DOX-loaded AuNR/R-SiO_2 sample (Fig. 9a). Meanwhile, after loading, the zeta potentials increased from −22.5 mV to +20.6 mV and the hydrodynamic diameters increased from 247 nm to 280 nm (Fig. S7†), which could confirm that DOX had been successfully loaded.

Fig. 9b shows that the loading amount of DOX increased linearly with the increase in original DOX concentrations. As the DOX concentrations changed from 0.125 to 1.5 mg mL^{-1}, the loading content increased from 183 mg g^{-1} to 2178 mg g^{-1}, and the loading efficiency did not considerably change, and still exceeded 73%. Therefore, the loading capacity in our study was extremely improved, almost 5 times than the classical mesoporous silica-coated AuNRs[17] and 2.4 times higher than the current rattle-type AuNR/porous-SiO_2.[26] It was reported that in order to improve the drug loading capacity, many post-treatment processes including surface-protected etching by PVP to achieve the hollow interiors of AuNR/SiO_2,[26] using H_2O_2 to fabricate rattle-shaped AuNR/mesoporous SiO_2,[42] were tried. Although the hollow interior can provide enough space for cargos, the drugs tend to be adsorbed just on the wall of the spheres. Contrary to the hollow structure in silica, the ultra-thick silica shell with a larger surface area and pore volume provides more absorption sites for guests, contributing to the high loading capacity.

3.6. Dual-stimulus drug release

Drug release behaviours of AuNR/R-SiO_2/DOX were studied with acidity and NIR laser stimuli (Fig. 10a and b). In the absence of 808 nm laser irradiation, the drug release rate was very slow, and only 6.8% of DOX was released (pH 7.4, 37 °C), and the release rate of DOX was accelerated when the pH of the PBS solution decreased to 5.0, up to 27.4%. This trend was attributed to the decreasing pH value that would reduce electrostatic binding and weaken the hydrogen bonds between DOX and mesoporous silica,[43] and hence accelerated the release in the acid solution (pH 5.0). In order to achieve faster release and "on-demand" release, NIR laser irradiation was performed repeatedly at the setting time points for 5 min and switched off for a while. Overall, this process was conducted for 7 cycles. It can be detected that when the NIR laser was on, the release rate of DOX was extremely improved. Once the light was switched off, the release rate would slow down immediately. After 7 on/off cycles, the cumulative DOX release was 24.9% at pH 7.4 and 78.3% at pH 5.0. Owing to the photothermal effect, the localized temperature raised after NIR laser irradiation, contributing to weaken the interaction between mesoporous silica shell and DOX. These results indicated that AuNR/R-SiO_2/DOX exhibited dual-stimulus-responsive drug-release behaviours (pH and NIR laser), and it could be finely controlled under the stimuli of an NIR laser on/off to achieve the "on-demand" release.

3.7. Cellular uptake and intracellular NIR-stimulated drug release

In this work, cellular uptake and intracellular NIR-stimulated drug release of AuNR/R-SiO_2/DOX were evaluated by CLSM. AuNRs can quench the red fluorescence signals of DOX when loaded in AuNR/R-SiO_2 (Fig. S8†). However, Fig. 11b shows a few red fluorescence signals after treatment with AuNR/R-SiO_2/DOX. These signals were attributed the unbound DOX, which were slowly released from AuNR/R-SiO_2/DOX under the stimuli of the intracellular acidic microenvironment. These images suggested that the HeLa cells could successfully internalize these nanoparticles. Under 808 nm laser irradiation, the red fluorescence signals were much stronger (Fig. 11c), indicating that the higher localized temperature could weaken the interactions between the drug and nanocarriers and accelerate the release rate of DOX, which are well consistent with our previous discussion.

3.8. Combined chemo-photothermal therapy

HeLa cells were the model cell systems to evaluate the *in vitro* cytotoxicity of the blank nanocarrier by CCK-8 assays. After incubation with different concentrations of AuNR/R-SiO_2 (even up to 400 μg mL^{-1}) for 24 h, the cell viabilities were still higher than 92% (Fig. 12a). Although CTAB as a stabilizer and soft template for preparing AuNR/R-SiO_2 is highly cytotoxic, after thermal annealing at high temperatures, CTAB decomposed thoroughly (Fig. S9†). This has contributed that nanocarriers become more biologically and clinically safe.

Last, the enhanced combined chemo-photothermal therapeutic efficiency of AuNR/R-SiO_2/DOX was also calculated by CCK-8 assays. HeLa cells were incubated with free DOX, AuNR/R-SiO_2, and AuNR/R-SiO_2/DOX for 4 h, and exposed to 808 nm laser irradiation for 5 min. After incubation for another 20 h, the cell viabilities were tested. As Fig. 12b shows, the dose-

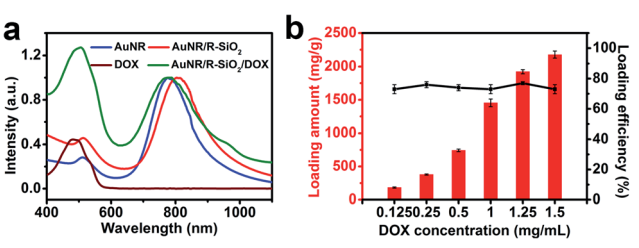

Fig. 9 (a) UV-vis-NIR spectra of DOX, AuNR, AuNR/R-SiO_2, and AuNR/R-SiO_2/DOX. (b) Loading capacity and loading efficiency of DOX.

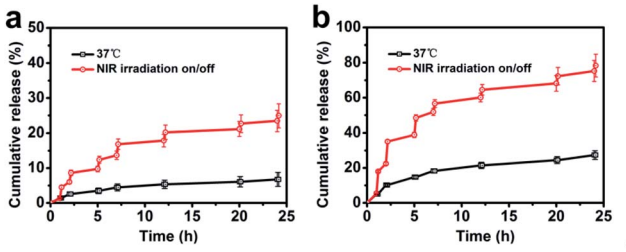

Fig. 10 Accumulated DOX release from AuNR/R-SiO_2/DOX in PBS at pH 7.4 (a) and 5.0 (b) at 37 °C. A 808 nm laser was used for irradiation at the setting points for 5 min.

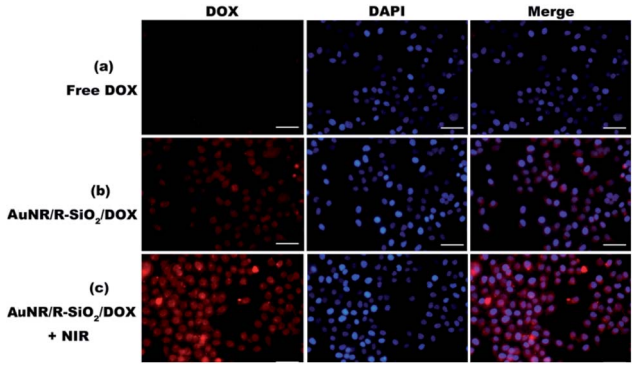

Fig. 11 Confocal fluorescence images exhibiting cellular uptake and intracellular NIR-stimulated DOX release in HeLa cells. (a and b) Without NIR laser irradiation; (c) with NIR laser irradiation (scale bar: 50 μm).

dependent therapeutic efficiency was exhibited in all HeLa cell lines. At a DOX concentration of 5 μg mL^{-1}, the cell viabilities of free DOX and AuNR/R-SiO_2/DOX were 18.3% and 42.5%, respectively. Compared with free DOX treatment only, the cell viability was higher when treated with AuNR/R-SiO_2/DOX. This finding indicated that the nanocarrier could effectively inhibit the fast and free releasing behaviours of DOX to achieve controllable release. Besides, when exposed to NIR laser irradiation after treatment with AuNR/R-SiO_2 only, the cell viability decreased remarkably (18.83%, with the equivalent DOX concentrations of 5 μg mL^{-1}), which was attributed to heat generated by AuNR/R-SiO_2. These results of single photothermal therapy were better than the similar report (80% [27] and 70%,[26] with the equivalent DOX concentrations of 5 μg mL^{-1}). More importantly, after incubation with AuNR/R-SiO_2/DOX and 808 nm laser irradiation for 5 min, the cell killing effects were enhanced significantly in all cell lines, even decreased to 9.29% at a DOX concentration of 5 μg mL^{-1}, better than others (40% [27] and 70%,[26] with the equivalent DOX concentrations of 5 μg mL^{-1}). These allow the conclusion that compared with a single therapy, combined chemo-photothermal therapy strategy exhibits better therapeutic effects and could be enhanced when taking AuNR/R-SiO_2 as the nano-drug carrier. As discussed, this is due to the fact as follows: (1) hyperthermia resulting from AuNRs under NIR laser irradiation could destroy cancer cells directly.[44,45] (2) Local heat could promote the DOX release to enhance the chemo-therapy effect. (3) Heating might enhance the cytotoxicity of DOX.[19,46] This study reveals that AuNR/R-SiO_2 offer exciting opportunities to reach the objective of enhanced combined photothermal-chemo therapy.

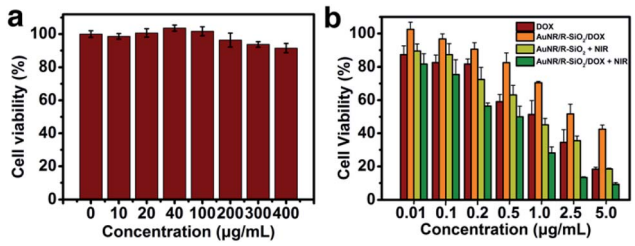

Fig. 12 (a) Evaluation of cytotoxicity at different concentrations of AuNR/R-SiO_2. (b) Evaluation of HeLa cells for therapy after incubation with different concentrations of free DOX, AuNR/R-SiO_2, and AuNR/R-SiO_2/DOX with or without NIR irradiation.

4 Conclusions

In summary, gold nanorods embedded in ultra-thick silica shells with radial mesopores (AuNR/R-SiO_2) have been successfully prepared. The shell thickness was up to ~83 nm with larger pores (~4.8 nm). Thanks to the ultra-thick shell, AuNR/R-SiO_2 exhibited ultra-high thermal stability, which could retain the integrity and photothermal effects even after heating at 800 °C and the change in the LSPR peak was a linear variation with the heating temperature from 400 to 800 °C ($y = -0.1045x + 901.7$, $R^2 = 0.997$). When taken as the nano-drug carrier, the treatment effect of the combined chemo-photothermal therapy was significantly enhanced for the following reasons: (1) owing to the thicker shell thickness, the loading capacity of doxorubicin (DOX) in the AuNR/R-SiO_2 spheres was relatively high as 2178 mg g^{-1}, almost 2.4–5.0 times higher than that in the similar reports. The injection dose of nano-drug carriers would be significantly less at equivalent concentrations of DOX, decreasing the risk of therapy. (2) Due to the mesopore structure of the SiO_2 shell, the photothermal effects of AuNRs could be significantly enhanced. When treated only with AuNR/R-SiO_2, the cell viability would be lower than that of others after NIR laser irradiation. (3) An ultra-thick shell can enhance the shape stability and thermal stability of AuNRs to achieve repeated photothermal therapy without the degradation of photothermal effects. This will improve the utilization of nano-drug carriers and achieve sustained release of drugs.

Beyond that, the release behaviours could be nicely controlled by acidity and near-infrared (NIR) laser, achieving drug release on demand. Furthermore, this nanocarrier was easy to be internalized by HeLa cells and had good biocompatibility. The AuNR/R-SiO_2/DOX exhibited enhanced combined chemo-photothermal therapy, displaying a higher therapeutic efficiency. These results present that AuNRs with ultra-thick silica shells could be applied as a dual-stimuli-responsive (pH/NIR) drug delivery system for cancer therapy. Future research should further develop and confirm these initial findings by widening the application range of AuNR/R-SiO_2.

Author contributions

Chun Shan: conceptualization, investigation, methodology, software, formal analysis, data curation, writing – original draft. Yuting Huang: investigation, resources, methodology, data curation. Junhao Wei: methodology, data curation. Min Chen: writing – review & editing, project administration, supervision, funding acquisition. Limin Wu: supervision, funding acquisition.

Conflicts of interest

There is no conflict of interest to declare.

Acknowledgements

Financial supports for this research are from the National Natural Science Foundation of China (51673041) and National Key Research and Development Program of China (2017YFA0204600, 2018YFE0201701).

Notes and references

1 G. Liu, H. Liang, Y. He, L. Lu, L. Wang, P. Liu and K. Cai, *J. Mater. Chem. B*, 2020, **8**, 9686–9696.
2 K. Shen, Y. Huang, Q. Li, M. Chen and L. Wu, *ACS Omega*, 2019, **4**, 18118–18125.
3 S. Debela, B. Mesfin and T. Senbeta, *Photonics Nanostructures: Fundam. Appl*, 2019, **33**, 48–54.
4 J. Li, H. Duan and K. Pu, *Adv. Mater.*, 2019, **31**, 1901607.
5 G. Hong, A. L. Antaris and H. Dai, *Nat. Biomed. Eng.*, 2017, **1**, 0010.
6 H. Petrova, J. P. Juste, I. Pastoriza-Santos, G. V. Hartland, L. M. Liz-Marzan and P. Mulvaney, *Phys. Chem. Chem. Phys.*, 2006, **8**, 814–821.
7 A. Antonello, E. Della Gaspera, J. Baldauf, G. Mattei and A. Martucci, *J. Mater. Chem.*, 2011, **21**, 13074–13078.
8 C.-S. Chang and L. J. Rothberg, *Chem. Mater.*, 2015, **27**, 3211–3215.
9 N. A. Joy, B. K. Janiszewski, S. Novak, T. W. Johnson, S.-H. Oh, A. Raghunathan, J. Hartley and M. A. Carpenter, *J. Phys. Chem. C*, 2013, **117**, 11718–11724.
10 V. Shanmugam, S. Selvakumar and C.-S. Yeh, *Chem. Soc. Rev.*, 2014, **43**, 6254–6287.
11 R. Di Corato, A. Espinosa, L. Lartigue, M. Tharaud, S. Chat, T. Pellegrino, C. Ménager, F. Gazeau and C. Wilhelm, *Biomaterials*, 2014, **35**, 6400–6411.
12 D. Soukup, S. Moise, E. Céspedes, J. Dobson and N. D. Telling, *ACS Nano*, 2015, **9**, 231–240.
13 D. Wu, X. Chen, J. Zhou, Y. Chen, T. Wan, Y. Wang, A. Lin, Y. Ruan, Z. Chen, X. Song, W. Fang, H. Duan and Y. Ping, *Mater. Horiz.*, 2020, **7**, 2929–2935.
14 Y. Li, X. Zhang, Z. Zhang, H. Wu, X. Xu and Z. Gu, *Mater. Horiz.*, 2018, **5**, 1047–1057.
15 T. Hashimoto, E. Yuba, A. Harada and K. Kono, *J. Mater. Chem. B*, 2020, **8**, 2826–2833.
16 J. Liu, C. Detrembleur, M.-C. De Pauw-Gillet, S. Mornet, C. Jerome and E. Duguet, *Small*, 2015, **11**, 2323–2332.
17 Z. Zhang, L. Wang, J. Wang, X. Jiang, X. Li, Z. Hu, Y. Ji, X. Wu and C. Chen, *Adv. Mater.*, 2012, **24**, 1418–1423.
18 J.-Y. Zeng, M.-K. Zhang, M.-Y. Peng, D. Gong and X.-Z. Zhang, *Adv. Funct. Mater.*, 2018, **28**, 1705451.
19 Y. Li, J. Jin, D. Wang, J. Lv, K. Hou, Y. Liu, C. Chen and Z. Tang, *Nano Res.*, 2018, **11**, 3294–3305.
20 A. Taruttis, N. Lozano, A. Nunes, D. A. Jasim, N. Beziere, E. Herzog, K. Kostarelos and V. Ntziachristos, *Nanoscale*, 2014, **6**, 13451–13456.
21 T. Wang, Y. Song, W. Zhang, Z. Wu, F. Li, Y. Su, Y. Yang, F. Li, P. Chen, J. Wang, Q. Wu, X. Sun, Y. Lu and D. Ling, *J. Biomed. Nanotechnol.*, 2017, **13**, 1435–1445.
22 M. Manzano and M. Vallet-Regí, *Adv. Funct. Mater.*, 2020, **30**, 1902634.
23 Y. Huang, K. Shen, Y. Si, C. Shan, H. Guo, M. Chen and L. Wu, *J. Colloid Interface Sci.*, 2021, **583**, 166–177.
24 Y. Si, M. Chen and L. Wu, *Chem. Soc. Rev.*, 2016, **45**, 690–714.
25 I. Gorelikov and N. Matsuura, *Nano Lett.*, 2008, **8**, 369–373.
26 Y. Yu, M. Zhou, W. Zhang, L. Huang, D. Miao, H. Zhu and G. Su, *Mol. Pharm.*, 2019, **16**, 1929–1938.
27 J. Wang, W. Zhang, S. Li, D. Miao, G. Qian and G. Su, *Langmuir*, 2019, **35**, 14238–14247.
28 M. N. Sanz-Ortiz, K. Sentosun, S. Bals and L. M. Liz-Marzan, *ACS Nano*, 2015, **9**, 10489–10497.
29 D. K. Roper, W. Ahn and M. Hoepfner, *J. Phys. Chem. C*, 2007, **111**, 3636–3641.
30 M. Lin, C. Guo, J. Li, D. Zhou, K. Liu, X. Zhang, T. Xu, H. Zhang, L. Wang and B. Yang, *ACS Appl. Mater. Interfaces*, 2014, **6**, 5860–5868.
31 S. Wang, M. Chen and L. Wu, *ACS Appl. Mater. Interfaces*, 2016, **8**, 33316–33325.
32 Q. Li, M. Chen, D. Chen and L. Wu, *Chem. Mater.*, 2016, **28**, 6584–6590.
33 K.-D. Shim and E.-S. Jang, *Bull. Korean Chem. Soc.*, 2018, **39**, 936–940.
34 A. Sinha and N. R. Jana, *Eur. J. Inorg. Chem.*, 2012, 4470–4478, DOI: 10.1002/ejic.201200496.
35 S. Lee, L. J. E. Anderson, C. M. Payne and J. H. Hafner, *Langmuir*, 2011, **27**, 14748–14756.
36 X. Li, T. Zhao, Y. Lu, P. Wang, A. M. El-Toni, F. Zhang and D. Zhao, *Adv. Mater.*, 2017, **29**, 1701652.
37 W.-C. Wu and J. B. Tracy, *Chem. Mater.*, 2015, **27**, 2888–2894.
38 M. Li, L. Li, K. Su, X. Liu, T. Zhang, Y. Liang, D. Jing, X. Yang, D. Zheng, Z. Cui, Z. Li, S. Zhu, K. W. K. Yeung, Y. Zheng, X. Wang and S. Wu, *Adv. Sci.*, 2019, **6**, 1900599.
39 W.-H. Chen, G.-F. Luo, Q. Lei, S. Hong, W.-X. Qiu, L.-H. Liu, S.-X. Cheng and X.-Z. Zhang, *ACS Nano*, 2017, **11**, 1419–1431.
40 N. N. M. Adnan, Y. Y. Cheng, N. M. N. Ong, T. T. Kamaruddin, E. Rozlan, T. W. Schmidt, H. T. T. Duong and C. Boyer, *Polym. Chem.*, 2016, **7**, 2888–2903.
41 S. Khashan, S. Dagher, S. Al Omari, N. Tit, E. Elnajjar, B. Mathew and A. Hilal-Alnaqbi, *Mater. Res. Express*, 2017, **4**, 055701.
42 E. Choi, M. Kwak, B. Jang and Y. Piao, *Nanoscale*, 2013, **5**, 151–154.
43 J. Zhu, L. Liao, X. Bian, J. Kong, P. Yang and B. Liu, *Small*, 2012, **8**, 2715–2720.
44 Z. Li, P. Huang, X. Zhang, J. Lin, S. Yang, B. Liu, F. Gao, P. Xi, Q. Ren and D. Cui, *Mol. Pharm.*, 2010, **7**, 94–104.
45 H.-C. Huang, K. Rege and J. J. Heys, *ACS Nano*, 2010, **4**, 2892–2900.
46 W. Zhang, Z. Guo, D. Huang, Z. Liu, X. Guo and H. Zhong, *Biomaterials*, 2011, **32**, 8555–8561.